Listening to ultrasound from plants reveals xylem vessel anatomy

Satadal Dutta (s.dutta-1@tudelft.nl)
TU Delft https://orcid.org/0000-0002-5817-5503
Elias Kaiser
Wageningen University and Research
Priscila Matamoros
Wageningen University and Research
Peter Steeneken
Delft University of Technology https://orcid.org/0000-0002-5764-1218
Gerard Verbiest
Delft University of Technology

Article

Keywords: xylem vessel anatomy, ultrasound,

Posted Date: May 10th, 2021

DOI: https://doi.org/10.21203/rs.3.rs-452046/v1

Listening to ultrasound from plants reveals xylem vessel anatomy

Satadal Dutta[1*], Elias Kaiser[2], Priscila M. Matamoros[2], Peter G. Steeneken[1], and Gerard J. Verbiest[1*]

[1]*Department of Precision and Microsystems Engineering, Faculty of 3ME, TU Delft, Mekelweg 2, 2628CD Delft, the Netherlands.*

[2]*Horticulture and Product Physiology, Department of Plant Sciences, Wageningen University and Research, Droevendaalsesteeg 1, 6708PB Wageningen, the Netherlands.*

Plants emit ultrasound pulses under drought stress, which originate in their water-carrying xylem vessels, and can be recorded externally. We demonstrate that these ultrasound pulses consist of superposed damped oscillations at plant-specific frequencies in the range of 10 – 150 kHz, that are correlated to xylem dimensions. We present a method to relate geometrical and viscoelastic properties of xylem vessels with the time- and frequency-domain characteristics of the observed oscillations. We apply the method to ultrasound pulses from drying shoots of three vascular dicot plant species. The extracted parameters are validated with destructive measurements of xylem vessel radii, wall thickness, length of xylem vessel elements, and the elastic modulus of the vascular bundle by optical and scanning cryo-electron microscopy and tensile loading. Our method demonstrates the potential for non-invasive and continuous monitoring of plant vascular anatomy. We foresee applications in high-throughput phenotyping and early detection of vascular wilt diseases.

Plant hydraulics, the study of water transport in plants, is vital to our understanding of plant function and stress resilience[1,2]. In vascular plants, the xylem is responsible for water and nutrient transport from the roots to the leaves[3]. Transpiration through leaves results in a tensile force on the water-column, which, combined with the strong cohesion of water molecules, results in ascent of water from the roots to the leaves[4]. During drought or strong transpiration rate, the tension in the water column increases rapidly. Beyond a critical tension, the stress is released by the formation of vapour or gas-bubbles [4-6] in the xylem. The bubble formation results in a sudden release of the elastic energy stored in the water column, a fraction of which is converted to a sound pulse[7]. The rate at which such pulses are emitted has been used as a marker of a plant's response and vulnerability to drought-stress [8-11]. The time- and frequency-domain features of these ultrasound pulses, measured directly from plant shoots, were shown in a recent study[12]. Yet, the physical origin and relevance of the observed damped oscillations in these acoustic pulses[13-16] has remained elusive.

Xylem vessels resemble cylindrical tubes with fused ends[3]. These tubes consist of several xylem vessel elements that are separated by perforation plates. Diameters of these vessels range from ~ 1 µm in small herbs to ~100 µm in woody trees, and their lengths range from ~100 µm to ~10 cm [17-19], across the plant kingdom. The viscoelastic walls of xylem cells are composed of an interwoven matrix of cellulose, hemicellulose, pectin and lignin fibres, which can have a wide range of elastic moduli depending on their relative composition[20] and the water content[21, 22]. The elasticity of macroscopic segments of plant stems can be measured via various mechanical loading techniques[23,24], which are invasive. Existing techniques to measure xylem dimensions, such as paint-injection, X-ray micro-CT, and optical and electron microscopy [25-28], are also destructive and time-consuming.

Here we present a physical model that links the dimensions and (visco-)elasticity of xylem vessels, to measured ultrasound pulses. We compare information about the radius, length, and viscoelasticity of xylem vessels obtained by analysing ultrasound pulses, to that gained by independent destructive techniques on *Hydrangea quercifolia*. In addition, the correlation between viscous damping in the ultrasound pulses and the vessel radius distribution is further elucidated by experiments on *Hydrangea macrophylla*., and *Solanum lycopersicum*. Lastly, via pulsed ultrasound spectroscopy with an external sound source, we show that acoustic resonances in the vascular tissue can be artificially excited, the characteristics of which agree with those excited naturally during drought-stress.

Results

Ultrasound waveforms. We first examined the waveforms of ultrasound pulses that were emitted by drying plant shoots. A total of three specimens, samples A, B, and C, were taken from three *H. quercifolia* plants (Methods). Ultrasound pulses were recorded with a broadband ultrasound microphone placed along the axial and radial direction of the stem (**Fig. 1a**). The microphone recorded the time series of the ultrasound emissions starting ~ 5 minutes into the drying process (**Fig. 1b**; Methods), where time $t = 0$ s corresponds to the start of the recording. The pulses occurred sporadically and with varying

amplitudes. We observed that the time-domain waveforms of these pulses resembled damped oscillations, both when recorded along the axial and in the radial directions (**Figs. 1c and 1d**). The pulse amplitude in time-domain decayed exponentially with a $1/e$ time constant τ_s: the settling time (Methods). For stem sample A, we extracted τ_s= 28.8 ± 6.4 µs (mean ± s.d.), for the pulses recorded in the axial direction. The corresponding value of τ_s for the radially recorded pulses was 41.7 ± 12.4 µs, which was statistically similar. The τ_s for the many individually measured axial and radial sound pulses of all the three stem samples A, B, and C are shown in **Supplementary Figs. 1 – 3,** respectively. The determined settling times of samples B and C agreed with those of sample A. All pulses died out within ~ 0.3 ms, in agreement with reported work[7]. Based on this observation, we hypothesize that the damped oscillations are generated by resonant vibrations within the xylem vessels. In the following paragraphs, the settling times and characteristic frequencies of ultrasound pulse waveforms were interpreted to estimate xylem vessel dimensions and elasticity (**Fig. 1e**).

Xylem vessel radius. In order to explain the origin of the observed ultrasound waveforms and to use them to extract information about the plant's microstructure, we develop a model relating the micromechanics of the xylem to the waveform of the generated ultrasound. We hypothesize that the damped oscillations are identical to those of an organ pipe filled with water[29]. The bubble formation excites axial standing waves in the sap (water), whose resonance frequencies depend on the longitudinal speed of sound in the pipe v_{eff}, and the xylem vessel element length L (Methods). We modelled the xylem vessel as a resonant cylindrical pipe containing a series network of vessel elements of length L, which are bounded by scalariform perforation plates[3, 25] (**Fig. 2a**). The perforation plates serve as non-ideal (leaky) reflecting surfaces at the termination of a vessel element for the pressure waves. The sound waves propagate along the length of the xylem vessel, and are likely to dominate the recorded ultrasound. These waves undergo damping, primarily due to the dynamic viscosity of sap (water) η_l in the xylem, which dominates the settling time τ_s. The resonating element can be described using a linear second order resonator model consisting of lumped acoustic inductance, capacitance and resistance (Methods). Using this acoustic model, we expressed the effective xylem radius in terms of the measured settling time using **equation** (**8**) (Methods), where ρ_l is the mass density of the sap (water). In this model, R can be calculated independently of length L, from the settling time of the measured time-domain waveform. The histograms of xylem radii R were extracted from the axially recorded ultrasound pulses, and also from optical micrographs of the stem samples (**Figs. 2d, Supplementary Fig. 4**). The mean (± s.d.) acoustic R for sample A was 9.93±1.6 µm. Similar values were obtained for stem samples B and C (**Supplementary Fig. 4**) Using optical micrographs of latex-paint stained transverse cross-sections of the stem sample A (**Fig. 2b**), we observed the vessel radius R = 11.9 ± 2.6 µm (**Fig. 2d and Table 1**). These values were confirmed with scanning electron cryo-microscopy (**Fig. 2c**). Thus, the calculated R, using the ultrasound analysis, agrees with that observed by optical and scanning electron microscopy.

We further validated our method using other plant species, namely *H. macrophylla* and *S. lycopersicum* (**Figs. 2e** – **2j**). The mean τ_s for *H. Macrophylla* and *S. lycopersicum* were 26.4±7.0 µs and 116±85.0 µs, respectively. Histograms and mean R derived from direct measurements (**Figs. 2g, 2h**), were in good agreement (**Figs. 2i, 2j**). The relatively larger τ_s for *S. lycopersicum* was in agreement with its wider mean vessel radius (20.4±7.1 µm), compared to that of *H. macrophylla* (10.9±2.4 µm). The corresponding vessel radii, obtained with the acoustic model, were 9.6±1.2 µm and 20.5±8.6 µm for the two species, respectively. The ultrasound methodology was thus validated for multiple plant species, showing the link between the vessel radii, and the settling time of the ultrasound pulses.

Xylem vessel (element) length and Young's modulus. To estimate the length L of the xylem vessel element, we analysed the frequencies in the ultrasound pulses. The resonance frequencies f_L are integer multiples of the ratio v_{eff} / L (Methods). We found that the Fourier spectra of representative ultrasound pulses (recorded axially) exhibited characteristic peak frequencies (**Fig. 3a**). The peak frequency with the largest amplitude, $f_{p(axial)}$ for sample A was 34±5 kHz. In addition, peaks close to integral multiples of $f_{p(axial)}$ were observed (**Supplementary Table 1**). Analysis of pulses from samples B and C showed similar trends (**Supplementary Fig. 5**). Similar data were observed in the pulses recorded in the radial direction of the stem samples (**Fig. 3b**, **Supplementary Fig. 5, Supplementary Table 2**).

The resonance frequency f_L was calculated from $f_{p(axial)}$ (**equation** (**6**); Methods). Note that the two values differ due to the high damping (small τ_s) in the sound pulse. To extract L from the resonance frequencies, we need the vessel wall thickness h and the Young's modulus of elasticity E (**equation** (**9**); Methods). We found h to be ~ 1 µm via scanning electron cryo-microscopy (**Fig. 2c**, Methods). We determined E of stem segments cut from the same plant, and from shoots similar in age and size. For this, we measured the stress-strain curves via uniaxial tensile loading (**Fig. 3c,** Methods). The mean mass density per stem segment was also estimated from the measured weights and dimensions. The linear slope of the stress-strain curve (**Fig. 3c**) at small values of strain ($\approx 10^{-4}$) yields the value of E, which was extracted to be 0.2 ± 0.1 GPa for fresh (hydrated) stem samples (**Fig. 3d**). For dry stem samples, E > 0.6 GPa were obtained. We observed an overall decline in E with increasing mass density. This indicates that the water-content dominates the variations in E. This agrees with an earlier empirical model[21], where the dependence of E on the relative water content in the xylem is taken into account.

We calculated L using $h \approx 1$ µm and E = 0.2±0.1 GPa (**equation** (**9**); Methods). The histogram of L was extracted from the axially recorded ultrasound pulses for stem samples. For sample A, L was 0.99±0.08 mm under a unimodal Gaussian fit (**Fig. 3e**). Similar values were obtained for samples B and C (**Supplementary Fig. 5**). This highlights the reproducibility of our method and the similarity of the recorded ultrasound pulses in the axial direction.

We validated the assumption that L represents the actual length of xylem vessel element. First, we extracted the mean xylem vessel length (a vessel contains several vessel elements) using latex paint staining[27], by counting the number of stained vessels on transverse cross-sections of the stem (Methods). These counts decrease exponentially with the distance[30] from the lower end of the stem at which the paint was taken up (**Supplementary Fig. 6**). The mean xylem vessel lengths were found to be in the range ~ 12 – 17 mm for the three stem samples. The xylem vessel length is thus much larger than the L extracted from the ultrasound pulses (~ 1 mm, **Fig. 3e**). This is because the Latex paint cannot penetrate the fused ends, but can pass through the perforation plates between adjacent vessel elements[30]. Next, we observed individual vessel elements in longitudinal sections of stem samples using scanning electron cryo-microscopy (**Fig. 3f**). The observed length ranged from 0.5 to 0.9 mm for individual xylem vessel elements (**Fig. 3g, Table 1**). Thus L, as obtained from our acoustic model, is a good estimate of the length of individual vessel elements.

Ultrasound pulsed transmission spectroscopy of xylem vessels. We further elucidated the observed link between the characteristics of drought-induced ultrasound pulses and the xylem vessel anatomy by artificially exciting ultrasonic resonances in the vascular tissue of a stem. A piezo-transducer transmits an acoustic pulse when excited electrically (Methods). This pulse was applied such that it propagated through a stem segment of *H. macrophylla* along either the axial or the radial direction, and was subsequently detected by the broad-band microphone (**Fig. 4a**). **Figures 4b and 4c** show the time-domain and frequency-domain waveform of the ultrasound pulse detected axially, while **Figs. 4d and 4e** show the same for the pulse detected radially. The ultrasound pulse exhibited an envelope settling time of 36.3 µs, which was in close agreement with that obtained from the drought-induced ultrasound pulses (26.4 ± 7.0 µs). In both axial and radial directions, characteristic frequencies were observed in the Fourier spectra, which match those observed in drought-induced pulses. This could enable the use of acoustic excitation as a technique for non-invasive monitoring of vascular geometry and moisture-dependent elasticity.

Discussion

Our results have shown how ultrasound emissions from drought-stressed plant stems can be used to extract and monitor the geometry and viscoelasticity of xylem vessels. In this section, we first interpret our results further and discuss the applicability of our method to monitor the vascular physiology of plants. We end the section by commenting on its potential in non-invasive plant health monitoring.

Xylem radius (*R*). We have shown that by modelling the xylem vessel as cylindrical acoustic resonator, the radius R can be extracted from the settling time of the ultrasound pulse, resulting in comparable values as those obtained from common microscopy techniques. Using *Hydrangea* and *Solanum* as example plant species with relatively narrow and wide vessel radii respectively, we validated the dependency of τ_s on R. Optically determined xylem vessel radii were slightly bigger (~ 2 µm) than the acoustically determined radii (**Figs. 2d**, **2i**, **2j**, **Supplementary Fig. 4**). We attribute this to the assumption of a constant dynamic viscosity of xylem sap η_l. In practice, η_l depends on ambient temperature, and concentration of dissolved nutrients[31]. Moreover, water close to the sap-wall interface is held with adhesive forces, and thus has a slightly higher dynamic viscosity[32]. As a corollary to our analysis, if the distribution of R is known directly from optical microscopy, one can evaluate the effective kinematic viscosity (η_l/ρ_l) of the xylem sap. Note that the solid walls of the xylem vessels also possess shear or extensional viscosity[33]. This means that elastic forces arise in them as a response to elongation, compression or shear stresses. Shear viscosity is a property of solids to resist a change in deformation (shear rate). This additional viscosity likely sets an upper bound on τ_s and R, beyond which the agreement between optical and acoustic radii likely deteriorates.

Xylem vessel element length (*L*) and Young's modulus (*E*). The xylem vessel element length L, extracted from the ultrasound pulses (**Fig. 3e**) consistently exceeded the physical length (via SEM; **Fig. 3g**) by ~ 0.3 mm (~ 30 %). We attribute this to two factors. Firstly, the perforation plates serve as non-rigid and leaky boundaries (not accounted for in the model), due to which the standing waves penetrate beyond the physical length of a single vessel element. Secondly, the uniaxial tensile loading measurements that we performed (**Fig. 3c, 3d**) on stems provide an overestimation of the xylem Young's modulus. This is due to the presence of stiffer Sclerenchyma and Collenchyma tissue[34], with Young's moduli exceeding ~ 1 GPa [35], close to the circumference of the stem. Hence, as a corollary to our analysis, instead of fixing the Young's modulus, one can alternatively fix the xylem vessel element length via microscopy. Xylem cells differentiate very early during the growth of a plant[36], subsequently growing to their maximum lengths before maturing (dying)[37] to become hydraulically active vessel elements. Thus, once the vessel element length is determined via microscopy techniques for a given plant, the Young's modulus can then be continuously and non-invasively monitored to diagnose variations in water-content[38], ageing, or even pathogen-induced occlusions within the xylem[39,40].

Relationship between *L* and *R*. Our method of analysing ultrasound emissions enabled us to generate a set of length versus radius data for xylem vessel elements within a given stem segment. We observed that in a single plant (*H. quercifolia*), L scales as $R^{0.74}$ (**Fig. 5**). Basic fluid and structural mechanics can help us in predicting an upper bound on L-R dependency. In plants of

height within ~1 m, transpiration pull is the governing force of ascent of water through xylem vessels, which creates a gradient in the hydrostatic pressure along the vascular column. With a constant volume flow rate of water through the series-connected vessel elements (continuity), the pressure-drop along a length L can be obtained from the Darcy-Weisbach equation[41] (Methods). Further, a vessel element can withstand a maximum pressure drop to avoid rupture (Methods)[42]. This critical pressure is also a function of both L and R. Combining the two dependencies, we can derive that $L_{\mathrm{crit}} \propto R^{1.25}$, where Young's modulus and wall thickness are assumed to be constants. This reasoning gives us an upper-bound on the scaling exponent from a purely mechanical viewpoint.

Application to intact plants. Plants vary in their drought-resistance. It may take several days for the water potential in the leaves to fall below the reported threshold[8] for cavitation based ultrasound emissions of at least one per minute. Therefore, we detached plant shoots to induce accelerated drought-stress. This enabled us to record a large set of ultrasound pulses in a relatively short time. We measured similar waveforms in both axial and radial directions of the stem. The latter direction avoids physical incision of the stem and is, therefore, preferred for non-invasive measurements on intact plants. Ultrasound does not propagate far and events occurring within a maximum distance of 20 – 30 mm are likely to be useful[43]. This distance depends on the species, and the level of hydration in the stem, and thus adjusting the proximity of the microphone to the stem may be necessary during growth or movements of the plant. For large trees/shrubs, the radius and lengths of the xylem vessels exceed ~100 µm, and ~10 cm. This would require shifting the sensitive frequency band of the microphone down to the audible range (100 Hz – 10 kHz).

Impact and scope. Despite centuries of research into plant hydraulics, our insights into xylem vessel properties and their influence on abiotic and biotic stress resilience, are still constantly evolving. This has largely been possible due to advancement in non-destructive measurement techniques to determine xylem vessel properties. Using methods like latex paint staining and scanning electron microscopy to monitor xylem vessels is time-consuming, and is of limited applicability in the field. Recently, X-ray micro-tomography was recommended[44] to monitor xylem embolisms and hydraulic vulnerability. However, to date, this method is expensive and not suitable for field applications. Ultrasound monitoring far surpasses these techniques, and has the potential to monitor xylem vessels non-destructively and continuously with a relatively inexpensive apparatus. The presented methodology establishes a link between geometrical and mechanical properties of xylem vessels and the recorded ultrasound emissions of plants. In particular, we showed, for the first time, the potential of ultrasound monitoring in the rapid determination of radius (R) and length (L) of xylem vessel elements in a single plant (**Fig. 5**). This opens the route to new studies about any existing physical relationship between L and R in a single plant. Note that although observed values of L and R were reported in literature[25,44,45], those were obtained only across different species by either destructive microscopy or X-ray micro-tomography.

We foresee applications of our method to a multitude of plant species with varying vessel dimensions and viscoelasticity. This can enable *in-vivo* studies to mechanical resonances of a plants' vascular tissue via external acoustic transducers. In turn, this provides a non-invasive method for rapid phenotyping. Crops could be selected for breeding based on their xylem vessels and thus based on their response to drought and/or susceptibility to vascular wilt pathogens[38,39,46,47]. Drought-stress directly impacts the viscoelasticity of the vascular tissue, which can be monitored with ultrasound. Correlation between vessel radius and drought-stress have been reported in poplar[48] and apple trees[49]. Pathogens within the xylem vessels have a parasitic effect on the sugar/nutrient concentration in the sap, which can in turn change the kinematic viscosity of the xylem sap.

Lastly, from the viewpoint of a complete sensor system, the presented methodology only uses Fourier transforms and envelope detection. These are standard signal processing functions, which can be implemented in commercial integrated chip (IC) technology. This will help with future development of low-cost and compact tools for monitoring plant stress. This will in turn boost climate-smart agriculture, and indoor farming by providing farmers with new tools for optimal irrigation strategies and early disease-detection.

Conclusions

We showed for the first time that the radius, length, and viscoelasticity of xylem vessel elements can be co-determined non-destructively and rapidly. This was achieved using a lumped mechanical model of the water-carrying xylem vessel. We analysed the time- and frequency-domain characteristics of ultrasound emission from drought-stressed stems of *Hydrangea quercifolia*. The ultrasound pulses were recorded along the radial and axial direction of stems using a broadband ultrasound microphone. A consistent set of characteristic peak frequencies across a multitude of ultrasound pulses in the range 10-150 kHz was observed. These remotely detected ultrasound pulses were attributed to damped acoustic resonances triggered by bubble formation inside the xylem vessels. We validated the model with results from common destructive methods of optical microscopy, latex paint-staining, scanning electron microscopy and tensile stress testing of plant stems. In particular, we showed that the mean settling time of the sound pulses increases with increasing mean xylem vessel radii through experiments on *Hydrangea macrophylla* and *Solanum lycopersicum*. As a further validation of our method, ultrasound pulsed transmission spectroscopy was performed on stem segments of *H. macrophylla*. A good agreement of the extracted settling time and the characteristic frequencies was obtained with those extracted from drought-induced sound pulses. The presented methodology provides a new outlook on plants "talking" during drought-stress, and presents ultrasound sensing as an inexpensive technique for rapid, non-invasive and in-vivo characterization of plant vasculature.

Methods

Plant material. Three potted plants of *Hydrangea quercifolia* were obtained from a commercial garden center and moved to the laboratory within 1 hour. One shoot sample per plant was cut, keeping the leaves intact, and immediately placed in tap water (**Supplementary Fig. 7**) to prevent embolism in the xylem vessels at the cut-end. From each shoot sample, a 60-70 mm long and trimmed (i.e., without leaves and petioles) stem segment was cut under water to prevent air entry and blockage. The segments were roughly cylindrical, with a cross-section diameter of ~ 5-6 mm, and were used for vessel staining and optical microscopy. The rest of the sample was left intact to measure ultrasound emissions. Additionally, one plant each of *Hydrangea macrophylla* and *Solanum lycopersicum*, was also obtained for optical microscopy and ultrasound recording.

Recording ultrasound pulses and signal processing. The shoot samples were taken out of water, dried using tissue paper, and left on the bench for air-drying, resulting in accelerated drought stress. A M500-USB ultrasound microphone, with a reliable detection window between 10 kHz and 150 kHz, from Pettersson Elektronik AB (Uppsala, Sweden) was placed first in the axial (~2 mm from the cut-face of stem normal to the cross-section) and then in the radial (on the cylindrical surface of the stem) directions (**Fig. 1a**) to record the ultrasound bursts at a sampling rate of 500 kHz in continuous time windows of 120 seconds. The sensor consists of a piezoelectric material which produces an electrical voltage proportional to the pressure of the incident sound wave. From the time-domain waveforms, the pulse envelope was obtained with the built-in "envelope ()" function in MATLAB, which returns the upper and lower envelopes of the input sequence, as the magnitude of its analytic signal. The analytic signal of the input sequence was found using the Hilbert transform. The peak of the envelope curve was determined and the decreasing part of the envelope curve was stored, which was subsequently fitted with the exponential function $\exp(-t/\tau_s)$ using the Least-Squares method. This yielded the settling time τ_s. The frequency spectra of the measured signals were obtained via a 250-point Discrete Fourier Transform, spanning a time frame of 1.5 ms. Due to the low intensity of the emitted sound, the spectra are shown until 150 kHz beyond which the signal merges with the noise floor of the sensor (- 80 dB). The raw data was then post-processed and analysed in MATLAB R2018b (MathWorks, Massachusetts, USA).

Analytical model for longitudinal vibrations. We modelled the xylem vessel as a cylindrical pipe of radius R, and effective length L sustaining longitudinal standing waves[50,51] in the water of density ρ_l whose resonance frequencies depend on the mode order m, and the longitudinal speed of sound in the pipe v_{eff}. The resonant frequency of the mth order (m = 1,2,…) is given by

$$f_m = \left(\frac{m}{2}\right)\frac{v_l}{L} \qquad (1)$$

where v_l is the speed of sound in the liquid (~1482 m/s in bulk water at 20 ºC). We denote the fundamental resonance frequency (m = 1) as f_L in the rest of this section. In practice, **equation (1)** cannot be applied directly because in a real pipe with an elastic wall, sound propagates at a slower speed than that in the bulk liquid. If the walls of the pipe have a non-zero acoustic thickness h and finite Young's modulus E, then the effective speed of sound is given by[52,53]:

$$\left(\frac{1}{v_{eff}^2}\right) = \left(\frac{1}{v_l^2}\right) + \rho_l\beta_{xylem}, \quad \text{where } \beta_{xylem} = \left(\frac{2R}{hE}\right) \qquad (2)$$

Where β_{xylem} is known as the cross-sectional compressibility, and ρ_l = 996 kg.m^{-3} is the mass density of water. Thus, v_l is replaced by v_{eff} in **equation (1)**.

These sound waves (expected to be dominant in the axially recorded ultrasound) undergo damping primarily due to the dynamic viscosity of water[54] η_l in the xylem. The resulting time-domain response of the resonating pipe can be described using a lumped circuit model consisting of acoustic inductance (L_a), capacitance (C_a) and resistance (R_a), analogous to an electrical L-C-R circuit, where voltage and current are replaced by pressure and flow rate respectively. L_a is a consequence of the kinetic energy in the water, while C_a arises due to the compressibility of water. R_a leads to energy dissipation and can be obtained from Poiseuille's law for capillary flow[33,50]. The three lumped parameters can be expressed as:

$$L_a = \frac{L.\rho_l}{\pi.R^2}, \qquad C_a = \frac{L.\pi.R^2}{\rho_l.v_l^2}, \qquad R_a = \frac{8.\eta_l.L}{\pi.R^4} \qquad (3)$$

where η_l = 8.9 x 10^{-4} Pa.s is the dynamic viscosity of water. By describing the circuit as a linear 2nd order differential equation, we obtained the damping ratio ζ, envelope settling time τ_s (the time needed for the amplitude to decrease by a factor of 'e'), and the driving frequency f_d as :

$$\zeta = \frac{R_a}{2}\sqrt{\frac{C_a}{L_a}} = \frac{4.\eta_l.L}{\rho_l.v_l.R^2} \qquad (4)$$

$$\tau_s = \frac{1}{\zeta.f_L} = \left(\frac{\rho_l}{4\eta_l}\right).R^2 \qquad (5)$$

$$f_d = f_L\sqrt{1-\zeta^2} \qquad (6)$$

The lumped model is valid as long as the dimensions L and R are smaller than the acoustic wavelength (~ 1-10 cm in water).

Noting that f_d is the same as the observed $f_{p(axial)}$ in the ultrasound pulses, ζ is obtained by combining **equations (5)** and **(6)** as :

$$\zeta = \frac{1}{\sqrt{1+\left(f_{p(axial)}.\tau_s\right)^2}} \qquad (7)$$

And the acoustic xylem radius was obtained by rearranging **equation (5)**:

$$R = \sqrt{\frac{4.\eta_l.\tau_s}{\rho_l}} \qquad (8)$$

Combining **equations (1)** and **(2)**, the effective xylem length L was obtained as:

$$\frac{1}{L^2} = \frac{4f_L^2}{m^2 v_{eff}^2} = \frac{4f_L^2}{m^2}\left[\frac{1}{v_l^2} + \frac{2\rho_l R}{h}.\left(\frac{1}{E}\right)\right] \qquad (9)$$

Scanning electron (cryo-) microscopy. Transverse sections from hydrangea stems were made using a razorblade. The cross-section was left on filter paper for 1-2 minutes to remove most of the adhering water. Thereafter, the section was fixed to a sample holder using Tissue-Tek. The sample was frozen by plunging the sample holder into liquid nitrogen. Subsequently the sample was transferred to a cryo-preparation chamber (Leica Microsystems, Wetzlar, Germany) under vacuum where it was kept at -90°C for 3 minutes to remove ice from the surface (freeze etching to remove water vapor contamination). While still under vacuum the sample was coated with 12 nm of tungsten and transferred using a VCT100 shuttle (Leica) to a field emission scanning electron microscope (Magellan 400 from FEI, Oregon, USA). The samples were analysed at 2 kV, 13 pA at -120°C.

Longitudinal sections were made by carefully cutting through the region that contains the xylem vessels. The rest of the sample preparation was identical.

Uniaxial tensile loading for Young's modulus determination. Multiple stem segments of lengths in the range of 4-7 cm were cut and mounted vertically between two clamps of a tensile testing machine (Z005; Zwick/Roell, Ulm, Germany; inset of **Fig. 3c**). The initial pre-strained length (l_0) is equal to the vertical separation between the clamps and was kept as 20 mm. The uniaxial stress was calculated as the tensile force applied by the equipment divided by the average cross-section area of the stem segment. The longitudinal strain was calculated as the change in stem length per unit initial length (Δl / l_0). The Young's modulus E was then extracted as the slope of the linear part of the stress-strain curve (Fig. 3c) at small values of strain ($\approx 10^{-4}$). The average mass density of each sample was also calculated from measured weight and volume just before tensile loading. The weights were measured with a Scaltec SBC 33 precision balance (Scaltec Instruments GmbH, Göttingen, Germany), while the dimensions were measured with a standard Vernier Calliper with a resolution of 0.1 mm. Note that the measurement error for elastic moduli and mass density (~ 20 %) is predominantly due to error propagation from length and diameter measurements.

Vessel staining and optical microscopy. An aqueous solution 1 % (v/v) suspension of red latex paint was left standing for at least 24 hours to allow large particles to settle at the bottom. The supernatant was subsequently transferred to a glass container and degassed. The stem segments were mounted vertically over the glass container, with one end immersed in the paint and the other end tightly inserted into a plastic tube connected to a suction pump (**Supplementary Fig. 7**) which applied a pressure difference of 400 mbar. The stem-tube junction was taped and smeared with Vaseline to prevent air leakage. As the solution was sucked through the stem for 12 hours, the paint remained confined in one xylem vessel (macromolecules in the paint cannot move through the bordering pits of xylem vessels) while the clear water was conducted through the entire stem. Subsequently, the stem samples were sliced with a blade at intervals of 5 mm. The number of painted vessels was then counted on each face of the cut slices from images (magnification of 200X) captured by a VHX digital microscope from Keyence.

An exponential relationship was observed[55] for the number of continuous xylem vessels at varying lengths of a stem segment. Typically, it is observed that longer vessels are also wider[56]. The complex relationship between xylem radius and length in a plant is largely affected by a trade-off between hydraulic conductance (increases with increasing R and decreasing L), and vulnerability to cavitation[57] (increases with increasing R and L). Sperry et al.[55,58] reported that the xylem vessel length has the following probability distribution function:

$$P(x) = x.\lambda_{xylem}^2 \exp(-\lambda_{xylem} x) \qquad (10)$$

Where the most probable vessel length is given by λ^{-1}_{xylem}, while the mean and standard deviation are respectively given by 2 λ^{-1}_{xylem}, and 1.414 λ^{-1}_{xylem}. **Equation (10)** is based on the assumption that xylem vessels have, for every additional unit length, a similar chance to terminate[55]. Thus, we describe the length distribution of a vessel population. Starting from a chosen reference position $x = 0$, the number of vessels N with length $L \geq x$ is given by

$$N = N_0 \exp(-\lambda_{xylem} x) \qquad (11)$$

Ultrasound pulsed transmission spectroscopy. A stem segment 43 mm in length and 5 mm in diameter was obtained from a *H. macrophylla* plant. For detecting axially transmitted ultrasound pulse through the stem, a piezo-transducer (MA40S4S; Murata Manufacturing Co., Ltd., Kyoto, Japan) with a resonant frequency of 40 kHz was excited with a voltage step of 10 V (zero offset), and an on-time of 500 ms. The transducer was placed perpendicular to one end of the stem segment. The M500-USB microphone was placed perpendicular to the other end of the stem segment. The frequency spectra of the measured signals were obtained via a 250-point Discrete Fourier Transform, spanning a time frame of 1.5 ms. The raw data was then post-processed and analysed in MATLAB R2018b (MathWorks, Massachusetts, USA). For radial transmission, the same stem segment was mounted between the transducer and the microphone such that the longitudinal axis of the stem was perpendicular to the line of flight of the sound pulse (**Fig. 4a**). The transducer was excited with a voltage step of 5 V and an on-time of 500 ms. The Fourier transform of the detected ultrasound pulse was performed over a time span of the first 100 µs (**Fig. 4d**), to observe the frequency components present in the pulse that propagated only through the stem.

Darcy-Weisbach equation and critical pressure in xylem vessel. The Darcy-Weisbach equation is an empirical relation that relates the pressure drop p along a given length L of a viscous and incompressible fluid flowing through a conduit of radius R as:

$$p = \frac{8\eta_l\, Q\, L}{\pi R^4} \qquad (12)$$

Where Q is the volumetric flow rate and η_l is the dynamic viscosity of the fluid (water).

From the viewpoint of mechanical rupture/failure, a biomechanical model was reported[42] where a vessel element is treated as a cylindrical shell under hydrostatic pressure of length L, radius R, uniform wall thickness t, and isotropic homogeneous Young's modulus E. For cylinders with $L/(R.t)^{0.5} > 4$ (applicable for xylem vessel elements), the critical hydrostatic pressure p_{crit} can be found from Batdorf's approximate formula[42, 59] as:

$$p_{crit} = \frac{0.92\ t^{5/2}\, E}{L.R^{3/2}} \qquad (13)$$

So, to prevent mechanical failure, $p < p_{crit}$. Substituting the above expressions and re-arranging the terms, we obtain:

$$L < \left(\sqrt{\frac{0.92\,\pi\, t^{5/2} E}{8\,\eta_l Q}}\right).R^{5/4} \qquad (14)$$

Data availability

The data that support the findings of this study are available from the corresponding author upon reasonable request.

References

1. McDowell, N.G., Brodribb, T.J. and Nardini, A. Hydraulics in the 21st century. *New Phytologist* **224**, 537–542 (2019).
2. Choat, B., Brodribb, T.J., Brodersen, C.R., Duursma, R.A., López, R. & Medlyn, B.E. Triggers of tree mortality under drought. *Nature* **558**, 531–539 (2018).
3. Venturas, M.D., Sperry, J.S. & Hacke, U.G. Plant xylem hydraulics: What we understand, current research, and future challenges. *J. Integr. Plant Biol.* **59(6)**, 356–389 (2017).
4. Zimmermann, U., Haase, A., Langbein, D., & Meinzer, F. Mechanisms of long-distance water transport in plants: a re-examination of some paradigms in the light of new evidence. *Phil.Trans. R. Soc. Lond. B* **341**, 19–31 (1993).
5. Caupin, F. & Herbert, E. Cavitation in water: a review. *C. R. Physique* **7**, 1000–1017 (2006).
6. Schenk, H.J., Steppe, K. & Jansen S. Nanobubbles: a new paradigm for air-seeding in xylem. *Trends in Plant Sci.* **20(4)**, 199–205 (2015).
7. Ponomarenko, A., Vincent, O., Pietriga, A., Cochard, H., Badel, É. & Marmottant, P. Ultrasonic emissions reveal individual cavitation bubbles in water-stressed wood. *J. R. Soc. Interface* **11**, 20140480 (2014).
8. Jackson, G.E., & Grace, J. Field measurements of xylem cavitation: are acoustic emissions useful? *J. Exp. Botany* **47(11)**, 1643–1650 (1996).
9. Rosner, S. Acoustic emission related to drought stress response of deciduous broad-leaved woody species. *J. Acoustic Emission* **30**, 11–20 (2012).
10. Nolf, M., Beikircher, B., Rosner, S., Nolf, A. & Mayr, S. Xylem cavitation resistance can be estimated based on time-dependent rate of acoustic emissions. *New Phytologist* **208**, 625–632 (2015).
11. Dostál, P., Sriwongras, P. & Trojan, V. Detection of acoustic emission characteristics of plant according to water stress condition. *Acta Univ. Agric. Silvic. Mendel. Brun.* **64(5)**, 1465–1471 (2016).
12. Oletic, D., Rosner, S., Zovko, M. & Bilas, V. Time-frequency features of grapevine's xylem acoustic emissions for detection of drought stress. *Computers and Electronics in Agriculture* **178**, 105797 (2020).
13. Ritman, K.T. & Milburn, J.A. Acoustic emissions from plants: ultrasonic and audible compared. *J. Exp. Botany* **39(9)**, 1237–1248 (1988).
14. Zweifel, R. & Zeugin F. Ultrasonic acoustic emissions in drought-stressed trees – more than signals from cavitation? *New Phytologist* **179**, 1070–1079 (2008).
15. Vergeynst, L.L., Sause, M.G.R., De Baerdemaeker, N.J.F., De Roo, L., & Steppe K. Clustering reveals cavitation-related acoustic emission signals from dehydrating branches. *Tree Physiology* **36,** 786–796 (2016).
16. Vergeynst, L.L., Sause, M.G.R., Hamstad, M.A. & Steppe K. Deciphering acoustic emission signals in drought stressed branches: the missing link between source and sensor. *Front. Plant Sci.* **6**:494 (2015).
17. Hacke, U.G., Spicer, R., Schreiber, S.G. & Plavcová, L. An ecophysiological and developmental perspective on variation of vessel diameter. *Plant Cell and Environment* **40**, 831–845 (2017).
18. Smith, M.S., Fridley, J.D., Yin, J. & Bauerle, T.L. Contrasting xylem vessel constraints on hydraulic conductivity between native and non-native woody understory species. *Front. Plant Sci.* **4**, 486 (2013).
19. Jacobsen, A.L., Pratt, R.B., Tobin, M.F., Hacke, U.G. & Ewers, F.W. A global analysis of xylem vessel length in woody plants. *Amer. J. Bot.* **99(10)**, 1583–1591 (2012).
20. Gibson, L.J. The hierarchical structure and mechanics of plant materials. *J. R. Soc. Interface* **9**, 2749–2766 (2012).
21. Niklas, K.J. Plant biomechanics: an engineering approach to plant form and function (The University of Chicago Press, 1992).
22. Schulgasser, K. & Witztum, A. On the strength of herbaceous vascular plant stems. *Annals of Botany* **80**, 35–44 (1997).
23. Niklas, K.J. & Moon, F.C. Flexural stiffness and modulus of elasticity of flower stalks from Allium stalks from Allium sativum as measured by multiple resonance frequency spectra. *Amer. J. Bot.* **75(10)**, 1517–1525 (1988).
24. Shah, D.U., Reynolds, T.P.S. & Ramage, M.H. The strength of plants: theory and experimental methods to measure the mechanical properties of stems. *J. Exp. Botany* **68(16)**, 4497–4516 (2017).

25. van der Schoot, C. & van Bel, A.J.E. Architecture of the internodal xylem of tomato (Solanum lycopersicum) with reference to longitudinal and lateral transfer. *Amer. J. Bot.* **76(4)**, 487–503 (1989).
26. Jacobsen, A.L. et al. Functional and ecological xylem anatomy: Grapevine xylem development, architecture, and function Ch. 5 (Springer International Publishing Switzerland, 2015).
27. Pen, R., Geng, J., Cai, J. & Tyree, M.T. A comparison of two methods for measuring vessel length in woody plants. *Plant, Cell, and Enviroment* **38**, 2519–2526 (2015).
28. Brodersen, C.R., Knipfer, T. & McElrone, A.J. *In-vivo* visualization of the final stages of xylem vessel refilling in grapevine (Vitis vinifera) stems. *New Phytologist* **217**, 117 – 126 (2018).
29. Angster, J., Rucz, P. & Miklós, A. Acoustics of organ pipes and future trends in the research. *Acoustics Today* **13(1)**, 10–18 (2017).
30. Ewers, F.W. and Fisher, J.B. Techniques for measuring vessel lengths and diameters in stems of woody plants. *Amer. J. Bot.* **76(5)**, 645–656 (1989).
31. Telis, V.R.N., Telis-Romero, J., Mazzotti, H.B. & Gabas, A.L. Viscosity of aqueous carbohydrate solutions at different temperatures and concentrations. *International Journal of Food Properties* **10(1)**, 185-195 (2007).
32. Goertz, M.P., Houston, J.E. & Zhu, X.-Y. Hydrophilicity and the viscosity of interfacial water. *Langmuir* **23**, 5491–5497 (2007).
33. Vogel, S. Life in moving fluids: The physical biology of flow (Princeton University Press, 1994).
34. Leroux, O. Collenchyma: a versatile mechanical tissue with dynamic cell walls. *Annals of Botany* **110**, 1083 – 1098 (2012).
35. Treitel, O. Elasticity of plant tissues. *Transactions of the Kansas Academy of Science* **47(2)**, 219 – 239 (1944).
36. Růžička, K., Ursache, R., Hejátko, J. & Helariutta, Y. Xylem development–from the cradle to the grave. *New Phytologist* **207(3)**, 519 – 535 (2015).
37. Jacobsen, A.L., Valdovinos-Ayala, J. & Pratt, R.B. Functional lifespans of xylem vessels: development, hydraulic function, and post-function of vessels in several species of woody plants. *Amer. J. Bot.* **105(2)**, 142 – 150 (2018).
38. von Arx, G., Archer, S.R. & Hughes, M.K. Long-term functional plasticity in plant hydraulic architecture in response to supplemental moisture. *Annals of Botany* **109**, 1091–1100 (2012).
39. Yadeta, K.A. & Thomma, B.P.H.J. The xylem as battleground for plant hosts and vascular wilt pathogens. *Front. Plant Sci.* **4: 97**, (2013).
40. Pouzoulet, J., Scudiero, E., Schiavon, M. & Rolshausen, P.E. Xylem vessel diameter affects the compartmentalization of the vascular pathogen *Phaeomoniella chlamydospora* in grapevine. *Front. Plant. Sci.* **8: 1442**, (2017).
41. Rouse, H. Elementary Mechanics of Fluids (New York: John Wiley & Sons Inc., 1946).
42. Karam, G.N. Biomechanical model of the xylem vessel elements in vascular plants. *Annals of Botany* **95**, 1179–1186 (2005).
43. Tyree, M.T. & Sperry, J.S. Characterization and propagation of acoustic emission signals in woody plants: towards an improved acoustic emission counter. *Plant, Cell, and Environment* **12**, 371–382 (1989).
44. Cochard, H., Delzon, S., Badel, E. X-ray microtomography (micro-CT): A reference technology for high-resolution quantification of xylem embolism in trees. *Plant Cell Environ*. **38**, 201–206 (2015).
45. Helmling, S., Olbrich, A., Heinz, I. & Koch, G. Atlas of vessel elements. *International Association of Wood Anatomists J.* **39(3)**, 249–352 (2018).
46. Blackman, C.J., Brodribb, T.J. & Jordan, G.J. Leaf hydraulic vulnerability is related to conduit dimensions and drought resistance across a diverse range of woody angiosperms. *New Phytologist* **188**, 1113–1123 (2010).
47. Haworth, M. et al. Xylem morphology determines the drought response of two *Arundo donax* ecotypes from contrasting habitats. *GCB Bioenergy* **9**, 119–131 (2017).
48. Arend, M. & Fromm, J. Seasonal change in the drought response of wood cell development in poplar. *Tree physiol.* **27**, 985 – 992 (2007).
49. Bauerle, T.L., Centinari, M. & Bauerle, W.L. Shifts in xylem vessel diameter and embolisms in grafted apple trees of differing rootstock growth potential in response to drought. *Planta* **234**, 1045–1054 (2011).

Additional references (Methods)

50. Kinsler, L.E, & Frey, A.R. Fundamentals of Acoustics, 2nd ed. (New York: John Wiley & Sons, 1962).
51. Wood, A. Acoustics, 2nd ed. (New York: Dover, 1966).
52. Tijsseling, A.S. Exact solution of linear hyperbolic four-equation system in axial liquid-pipe vibration. *J. Fluids and Structures* **18(2)**, 179–196 (2003).
53. Ghidaoui, M.S., Zhao, M., McInnis, D.A. and Axworthy, D.H. A review of water hammer theory and practice. *Appl. Mech. Rev.* **58(1)**, 49–76 (2005).
54. Aleksandrov, A.A. & Trakhtengerts, M.S. Viscosity of water at temperatures of -20 to 150 ºC. *J. Engineering Phys.* **27**, 1235–1239 (1974).
55. Nijsse, J. On the mechanism of xylem vessel length regulation. *Plant Physiology* **134(1)**, 32–34 (2004).
56. Hacke, U.G., Sperry, J.S., Wheeler, J.K. & Castro, L. Scaling of angiosperm xylem structure with safety and efficiency. *Tree Physiology* **26**, 689–701 (2006).
57. Ooeda, H., Terashima, I. and Taneda, H. Intra-specific trends in lumen and wall resistivities of vessels within the stem xylem vary among three woody plants. *Tree Physiology* **38**, 223–231 (2017).
58. Comstock, J.P. and Sperry, J.S. Theoretical considerations of optimal conduit length for water transport in vascular plants. *New Phytol.* **148**, 195–218 (2000).
59. Kollàr, L.& Dulàcska, E. Buckling of shells for engineers (New York: John Wiley & Sons Inc., 1984).

Acknowledgments

This work has been carried out under the “Plantenna” research programme, a collaboration among the members (technical universities) of the 4TU federation in the Netherlands. The authors would like to thank Lars Pettersson for technical support

concerning the ultrasound sensor equipment, dr. ing. Marcel Giesbers for support with scanning electron microscopy, and Patrick van Holst for technical support in measuring the stress-strain curves of the stem samples.

Author contributions

S.D. and G.V. conceived the idea. G.V., E.K., and P.G.S. supervised the work. S.D. performed the ultrasound measurements, elastic modulus measurements, and the analysis/modelling of data. E.K. obtained the plant specimens. P.M.M. and S.D. carried out the paint infusion method and analysed the microscopic images for determining vessel length and diameter. E.K. and P.M.M. provided necessary advice on plant physiology. S.D., and G.V. prepared the manuscript. E.K., P.G.S. and G.V. revised the manuscript. All authors read and approved the manuscript.

Competing interests

The authors declare no competing interests.

Corresponding authors ORCID iD:

https://orcid.org/0000-0002-5817-5503, (Email: s.dutta-1@tudelft.nl)

https://orcid.org/0000-0002-1712-1234, (Email: g.j.verbiest@tudelft.nl)

Additional information

Supplementary information is available for this paper.

Listening to ultrasound from plants reveals xylem vessel anatomy (Figures)

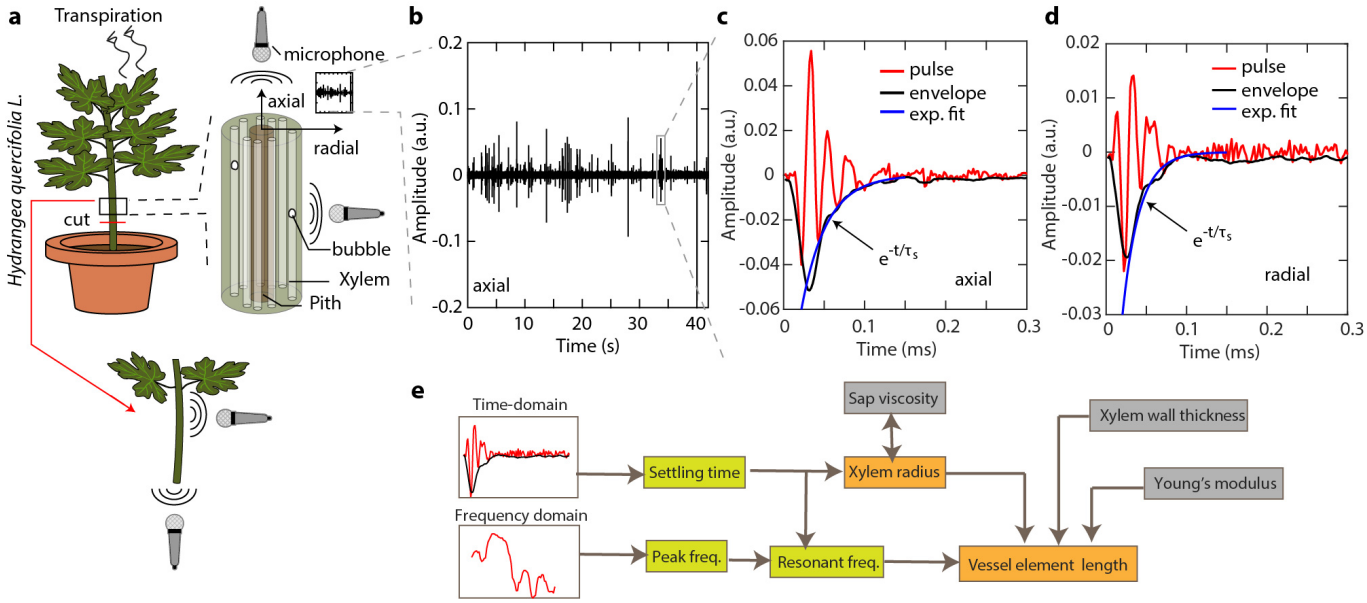

Figure 1: Ultrasound measurement set-up and time-domain signal. **(a)** Schematic set-up for recording of ultrasound pulses from shoots of *Hydrangea quercifolia* along axial and radial directions. The zoom-in represents a schematic of the vascular bundle of the stem, showing the peripheral arrangement of tubular xylem vessels around the pith in the core. Bubbles seeded in the vessels trigger the emission of ultrasound pulses. **(b)** Example raw time-domain data for ultrasound recorded along the axial direction of a stem. Time $t = 0$ represents the start of the recording, which occurs after ~ 5 minutes of drying. **(c), (d)** Zoomed-in time-domain example ultrasound pulses recorded axially and radially, respectively. Black curves represent the amplitude envelope that decays exponentially (damping), and blue curves represent the exponential fit of the envelope decay. **(e)** Schematic flow-chart illustrating the steps in our analysis. The settling time and peak frequencies are obtained from the time-domain and frequency-domain waveforms (**Figs. 2e, 2f, 3a, and 3b**). The resonant frequency is obtained from peak frequency and settling time (Methods, **equation (6)**). Using these, xylem radius and xylem vessel element length are extracted (**Table 1**). Parameters of sap viscosity, vessel wall-thickness and young's modulus are taken as input.

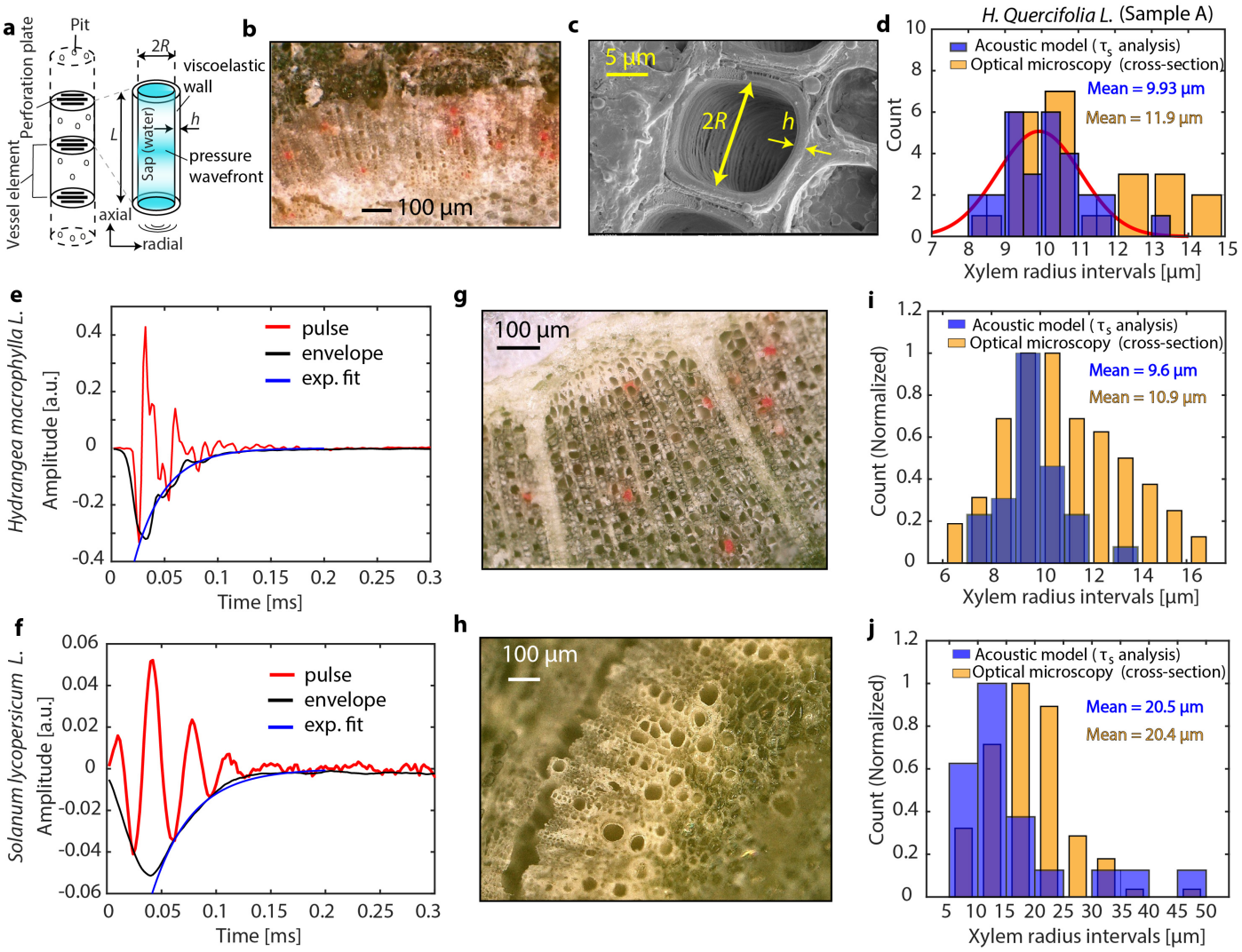

Figure 2: Xylem vessel radius extraction from damping in axial sound waves. (a) Schematic of water-conducting xylem vessels in vascular plants. Vessels are the dominant and more efficient cells to transport water in *H. quercifolia*. They consist of a series network of vessel members/elements, which are interconnected via perforation plates. Also shown is the simplified cylindrical acoustic-resonator model for a vessel element sustaining damped longitudinal standing waves in its sap, the damping factor being a function of sap viscosity and the radius of the vessel. **(b)** Optical micrograph of the transverse section of stem sample A, showing the xylem vessels filled with latex paint. **(c)** Cryo-SEM image of the transverse section of a stem sample showing the diameter (2*R*) and the wall thickness (*h*) of a xylem vessel. **(d)** Histogram showing the model-extracted xylem radii (in blue), and that of the observed xylem radii (in yellow) obtained via latex-staining and optical microscopy for stem sample A of *H. quercifolia*. The red curve represents a unimodal Gaussian fit. **(e),(f),(g)** Time-domain ultrasound waveform, cross-section optical micrograph (300X) of stem, and histograms of observed (in yellow) and acoustic (in blue) xylem vessel radii, respectively, in *H. macrophylla* stem sample recorded along the axial direction. **(h), (i), (j)** Time-domain ultrasound waveform, cross-section optical micrograph (200X) of stem, and histograms of observed (in yellow) and acoustic (in blue) xylem vessel radii, respectively, in *Solanum lycopersicum* stem sample recorded along the axial direction.

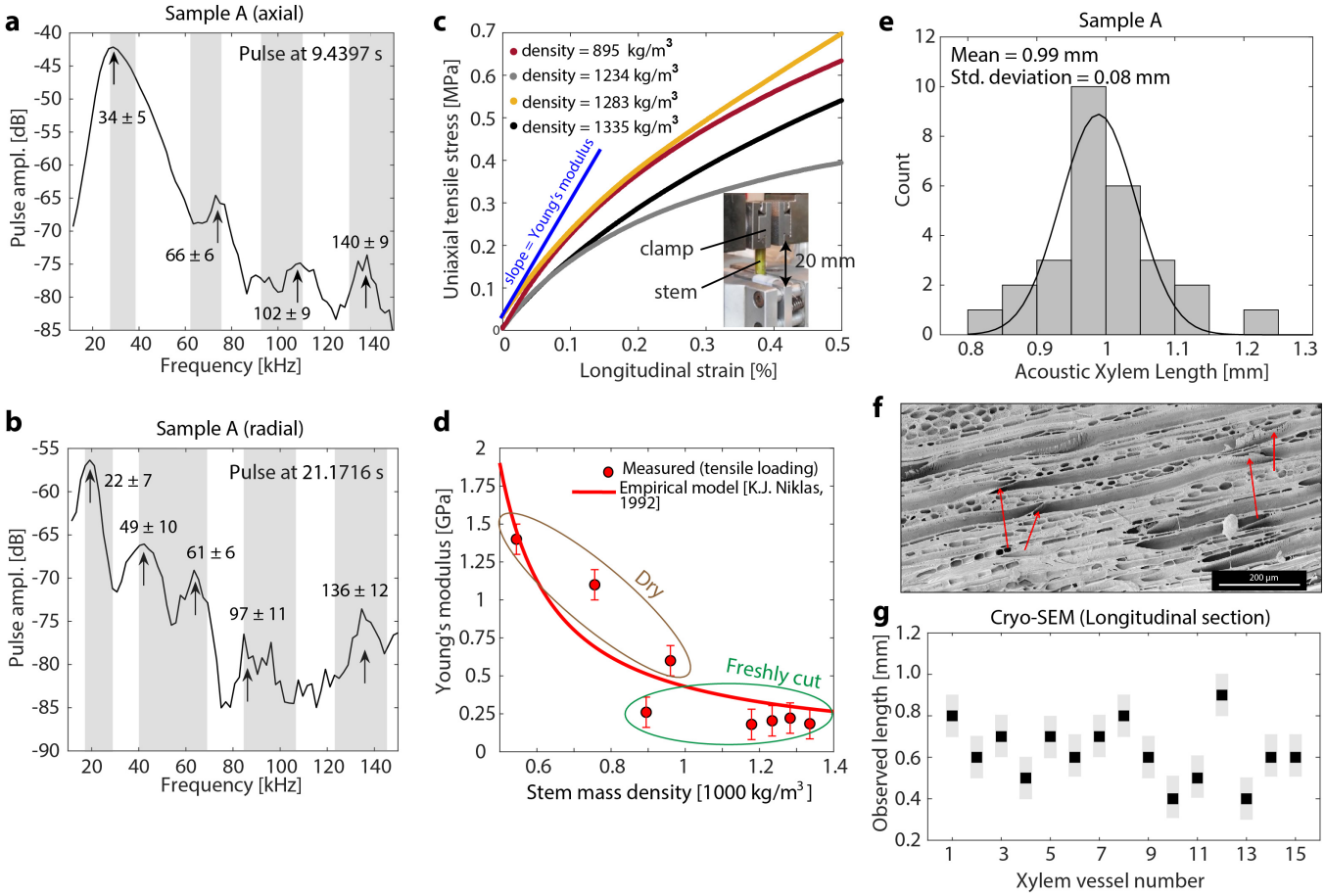

Figure 3: Ultrasound frequency spectra, Young's moduli of stem, and extraction of xylem vessel element lengths. (a), (b) Observed characteristic peak-frequencies in the example Fourier transform of the ultrasound pulses recorded axially and radially, respectively, in sample A of *H. quercifolia*. The black curve represents the spectrum of a representative pulse with the indicated timestamp of the recording. Grey shaded regions indicate the variation in the peak frequencies among the individual pulses (mean± standard deviation). **(c)** Measured stress-strain curve for freshly cut stem segments of *H. quercifolia* with mass densities indicated in the legend. The blue line represents the linear fit of a stress-strain curve at low strain, the slope of which, yields the Young's modulus in accordance with Hooke's Law. The inset shows the photograph of the set-up for uniaxial tensile loading of the stem. **(d)** Extracted Young's modulus versus mass density for freshly cut and dried stem segments, extracted from stress-strain measurements (solid circles) with indicated error bars (± 0.1 GPa). The red curve represents a fit based on the empirical model[21] of Young's moduli as a function of relative water-content in stems. **(e)** Histogram showing the extracted xylem vessel element lengths in stem sample A, extracted via the acoustic model. The black curve represents a unimodal Gaussian fit. **(f)** Example cryo-SEM image of the longitudinal section of a stem segment (*H. quercifolia*), showing the structure of individual vessel elements terminated by scalariform perforation plates (marked by red arrows). Observed length of each element is in the range 600 µm – 900 µm. **(g)** Scatter plot showing the observed length of xylem vessel elements via cryo-SEM technique. The grey bars indicate the upper and lower bounds due to the slant length of the perforation plates along the longitudinal axis (~ 100 µm).

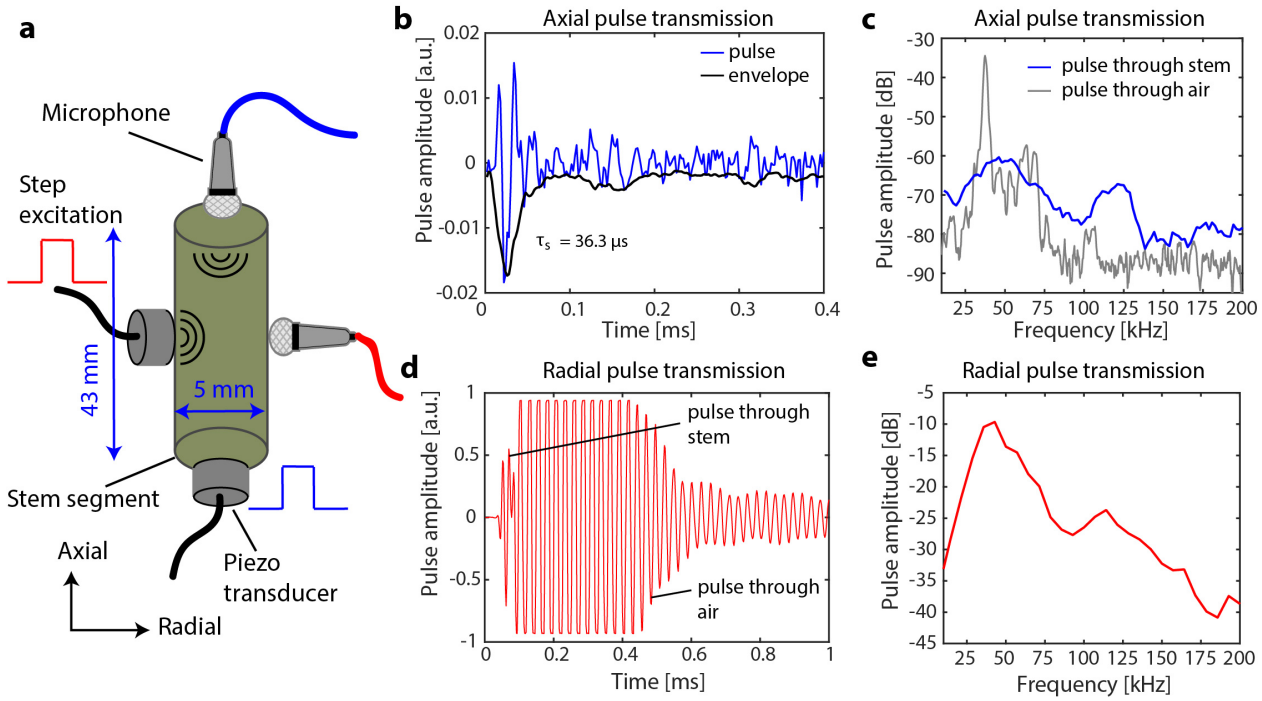

Figure 4: Ultrasound pulsed transmission spectroscopy of vascular tissue. (a) Schematic measurement set-up showing an external piezo-ultrasound transducer (resonant frequency of 40 kHz) and the broad-band microphone placed along the axial and radial direction to a *H. macrophylla* stem with the indicated dimensions. The piezo-transducer is excited with a voltage step in order to emit a broad-band acoustic pulse. **(b)** Time-domain waveform (in blue) with the fitted envelope, and **(c)** Fourier spectra of the axially transmitted sound pulse (in blue). The spectrum of the sound pulse emitted by the transducer (source) with transmission through air is shown in grey as a reference. **(d)** Time-domain waveform and **(e)** Fourier spectra of the radially transmitted sound pulse.

Table 1: Summary of extracted parameters via the ultrasound analysis for the three stem samples of *H. quercifolia*.

Parameter	**Ultrasound method**	**Destructive measurement**	
Xylem radii [µm]	9.89 ± 1.6	12.4 ± 2.6	Optical microscopy, Scanning electron microscopy
Mean Xylem vessel length [mm]	---	16.9 (sample A), 12.8 (sample B), 14.4 (sample C).	Latex-paint staining and vessel counting
Xylem vessel element length [mm]	0.98 ± 0.14	0.63 ± 0.14	Scanning electron microscopy
Young's modulus of elasticity [GPa]	---	0.2 ± 0.1	Uniaxial tensile loading

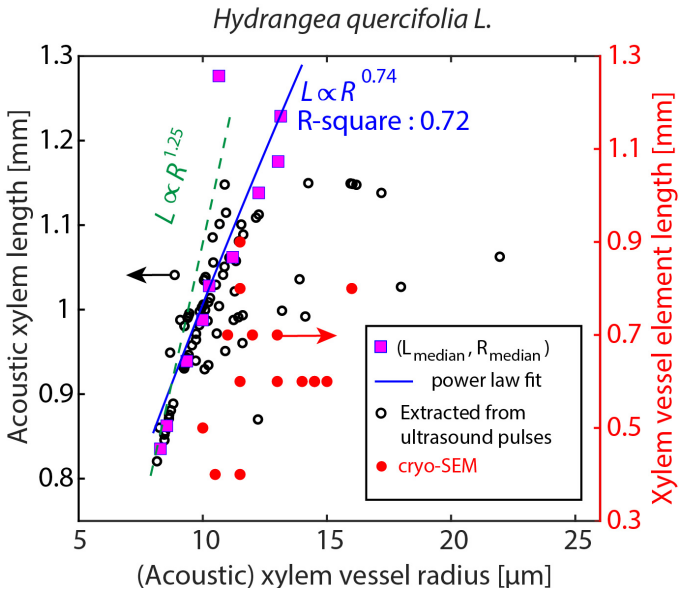

Figure 5: Acoustic xylem vessel element length versus vessel radius. Black circles: scatter plot of model-extracted (acoustic) xylem vessel element length (L) and radius (R) corresponding to each analysed ultrasound pulse. Data from all three stem samples of *H. quercifolia* are merged here. The radii were obtained from the settling time of the ultrasound pulses, while the lengths were obtained from the resonance frequency of the sound pulses and by measuring the Young's modulus (**Fig. 1e**). The data points are classified into bins of L with intervals of 0.5 mm. In each bin, the median L and R are calculated (pink squares), and fitted with a power law function (blue line). The green dashed line indicates the predicted L-R dependency in accordance with Darcy-Weisbach equation for fluid flow, combined with mechanical failure of the xylem vessel (Methods). Red circles: observed vessel element lengths and radius in *H. quercifolia* via cryo-SEM technique.

Figures

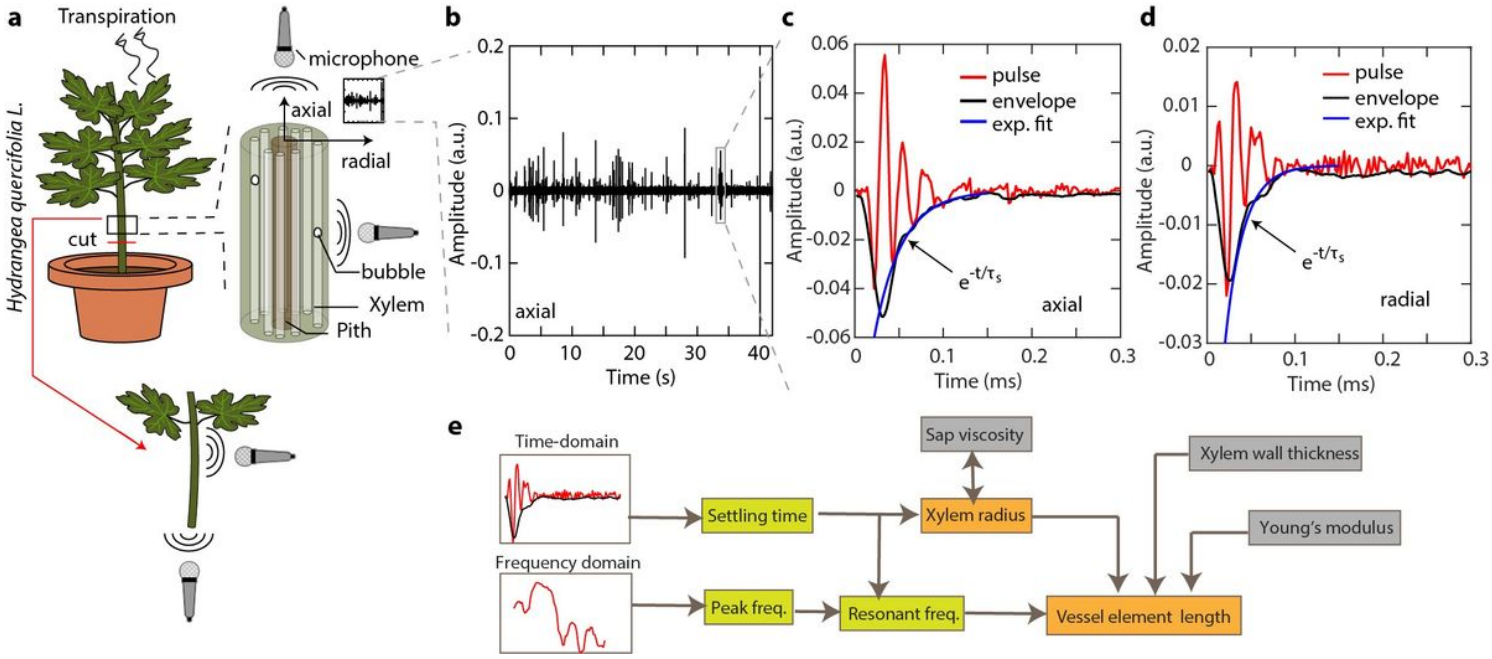

Figure 1

Ultrasound measurement set-up and time-domain signal. (a) Schematic set-up for recording of ultrasound pulses from shoots of Hydrangea quercifolia along axial and radial directions. The zoom-in represents a schematic of the vascular bundle of the stem, showing the peripheral arrangement of tubular xylem vessels around the pith in the core. Bubbles seeded in the vessels trigger the emission of ultrasound pulses. (b) Example raw time-domain data for ultrasound recorded along the axial direction of a stem. Time t = 0 represents the start of the recording, which occurs after ~ 5 minutes of drying. (c), (d) Zoomed-in time-domain example ultrasound pulses recorded axially and radially, respectively. Black curves represent the amplitude envelope that decays exponentially (damping), and blue curves represent the exponential fit of the envelope decay. (e) Schematic flow-chart illustrating the steps in our analysis. The settling time and peak frequencies are obtained from the time-domain and frequency-domain waveforms (Figs. 2e, 2f, 3a, and 3b). The resonant frequency is obtained from peak frequency and settling time (Methods, equation (6)). Using these, xylem radius and xylem vessel element length are extracted (Table 1). Parameters of sap viscosity, vessel wall-thickness and young's modulus are taken as input.

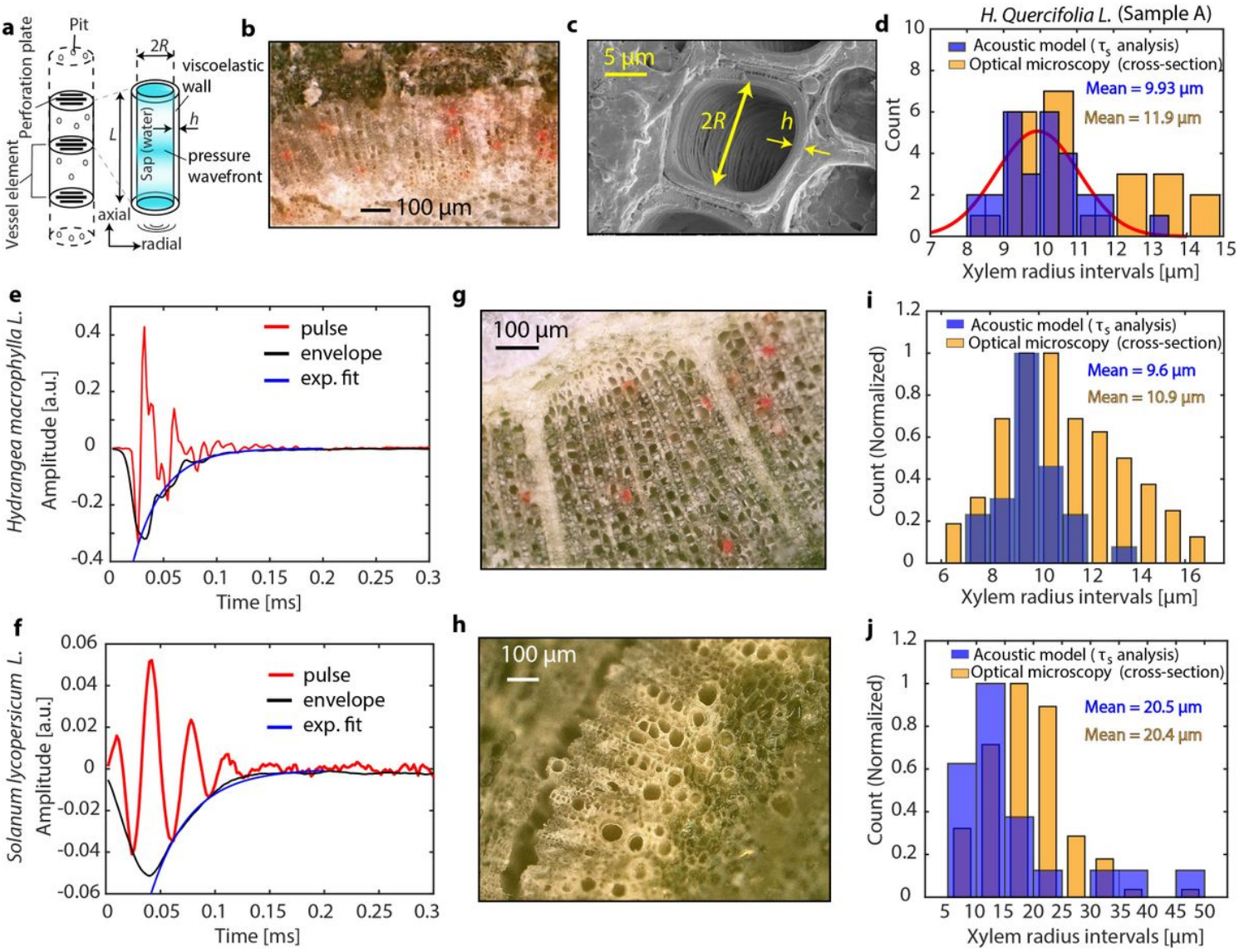

Figure 2

Xylem vessel radius extraction from damping in axial sound waves. (a) Schematic of water-conducting xylem vessels in vascular plants. Vessels are the dominant and more efficient cells to transport water in H. quercifolia. They consist of a series network of vessel members/elements, which are interconnected via perforation plates. Also shown is the simplified cylindrical acoustic-resonator model for a vessel element sustaining damped longitudinal standing waves in its sap, the damping factor being a function of sap viscosity and the radius of the vessel. (b) Optical micrograph of the transverse section of stem sample A, showing the xylem vessels filled with latex paint. (c) Cryo-SEM image of the transverse section of a stem sample showing the diameter (2R) and the wall thickness (h) of a xylem vessel. (d) Histogram showing the model-extracted xylem radii (in blue), and that of the observed xylem radii (in yellow) obtained via latex-staining and optical microscopy for stem sample A of H. quercifolia. The red curve represents a unimodal Gaussian fit. (e),(f),(g) Time-domain ultrasound waveform, cross-section optical micrograph (300X) of stem, and histograms of observed (in yellow) and acoustic (in blue) xylem vessel radii, respectively, in H. macrophylla stem sample recorded along the axial direction. (h), (i), (j) Time-

domain ultrasound waveform, cross-section optical micrograph (200X) of stem, and histograms of observed (in yellow) and acoustic (in blue) xylem vessel radii, respectively, in Solanum lycopersicum stem sample recorded along the axial direction.

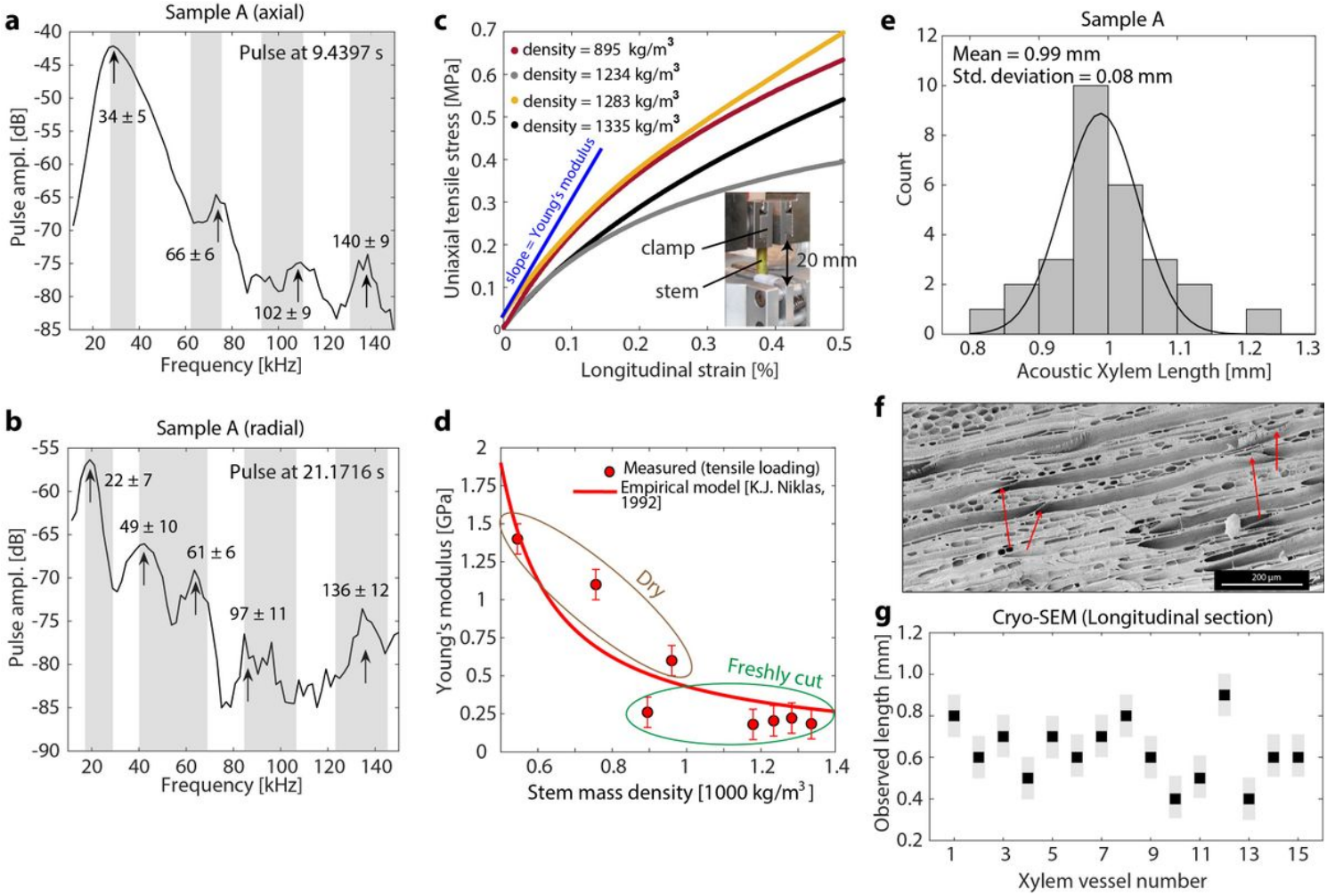

Figure 3

Ultrasound frequency spectra, Young's moduli of stem, and extraction of xylem vessel element lengths. (a), (b) Observed characteristic peak-frequencies in the example Fourier transform of the ultrasound pulses recorded axially and radially, respectively, in sample A of H. quercifolia. The black curve represents the spectrum of a representative pulse with the indicated timestamp of the recording. Grey shaded regions indicate the variation in the peak frequencies among the individual pulses (mean± standard deviation). (c) Measured stress-strain curve for freshly cut stem segments of H. quercifolia with mass densities indicated in the legend. The blue line represents the linear fit of a stress-strain curve at low strain, the slope of which, yields the Young's modulus in accordance with Hooke's Law. The inset shows the photograph of the set-up for uniaxial tensile loading of the stem. (d) Extracted Young's modulus versus mass density for freshly cut and dried stem segments, extracted from stress-strain measurements (solid circles) with indicated error bars (± 0.1 GPa). The red curve represents a fit based on the empirical model21 of Young's moduli as a function of relative water-content in stems. (e) Histogram showing the extracted xylem vessel element lengths in stem sample A, extracted via the acoustic model. The black

curve represents a unimodal Gaussian fit. (f) Example cryo-SEM image of the longitudinal section of a stem segment (H. quercifolia), showing the structure of individual vessel elements terminated by scalariform perforation plates (marked by red arrows). Observed length of each element is in the range 600 µm – 900 µm. (g) Scatter plot showing the observed length of xylem vessel elements via cryo-SEM technique. The grey bars indicate the upper and lower bounds due to the slant length of the perforation plates along the longitudinal axis (~ 100 µm).

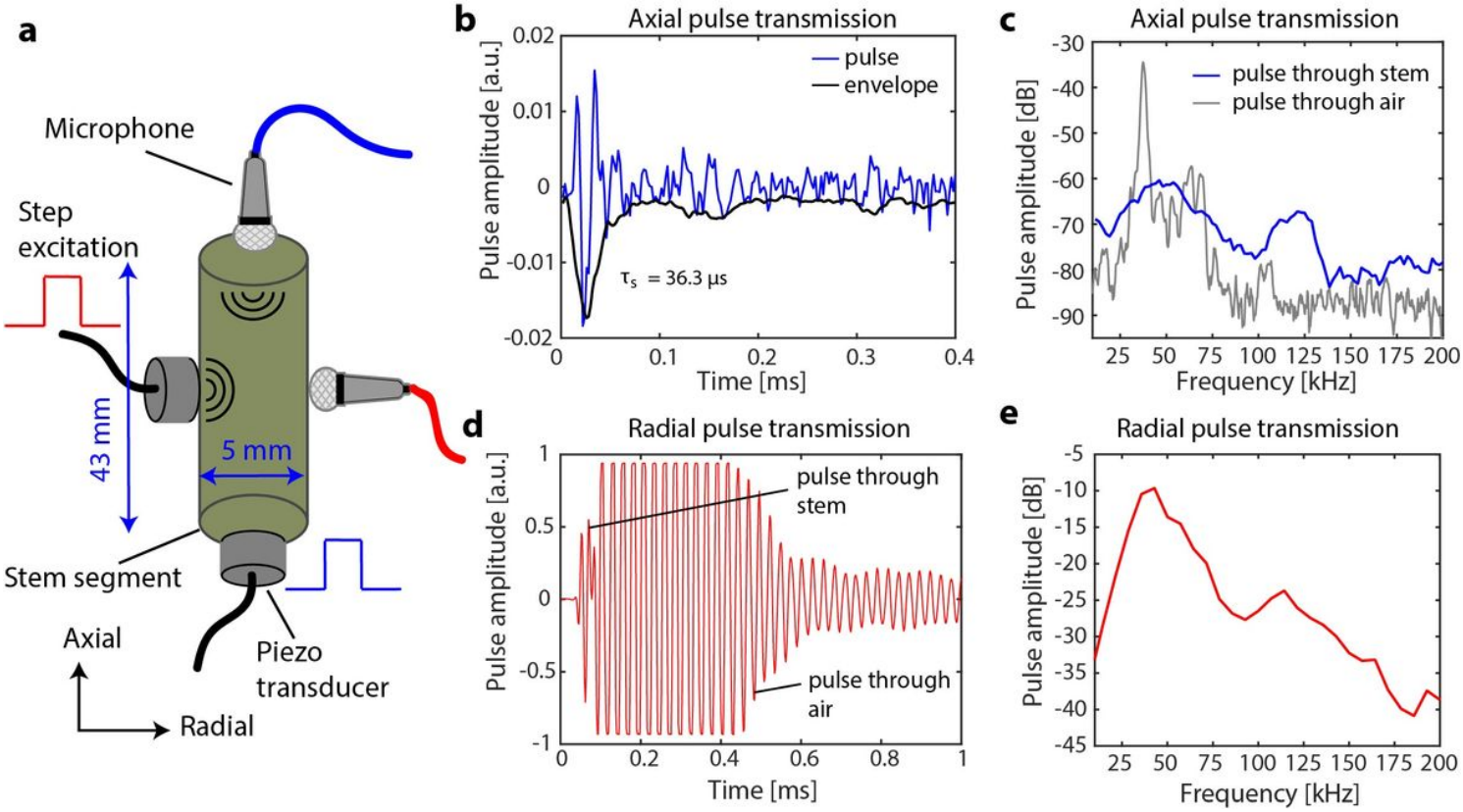

Figure 4

Ultrasound pulsed transmission spectroscopy of vascular tissue. (a) Schematic measurement set-up showing an external piezo-ultrasound transducer (resonant frequency of 40 kHz) and the broad-band microphone placed along the axial and radial direction to a H. macrophylla stem with the indicated dimensions. The piezo-transducer is excited with a voltage step in order to emit a broad-band acoustic pulse. (b) Time-domain waveform (in blue) with the fitted envelope, and (c) Fourier spectra of the axially transmitted sound pulse (in blue). The spectrum of the sound pulse emitted by the transducer (source) with transmission through air is shown in grey as a reference. (d) Time-domain waveform and (e) Fourier spectra of the radially transmitted sound pulse.

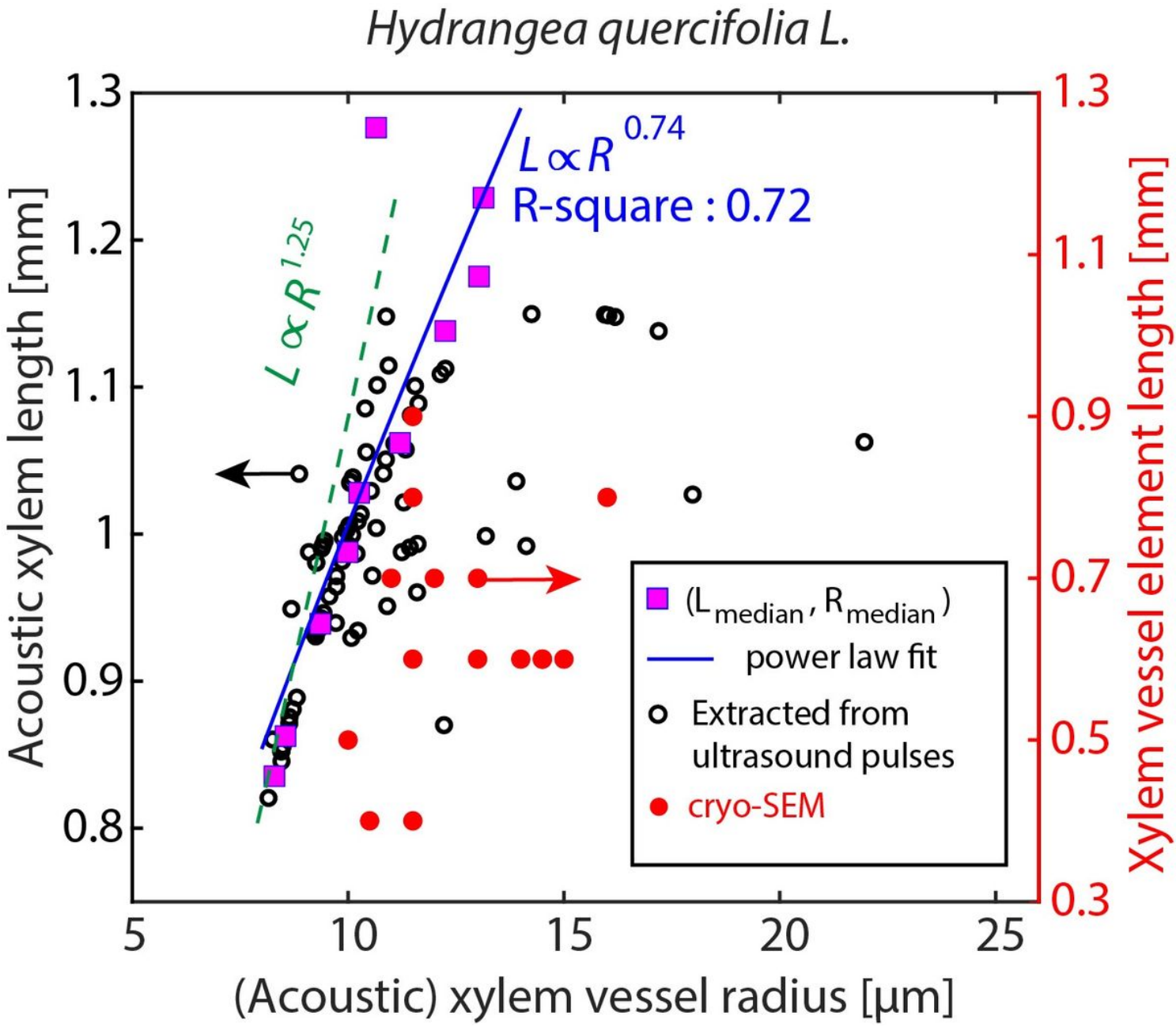

Figure 5

Acoustic xylem vessel element length versus vessel radius. Black circles: scatter plot of model-extracted (acoustic) xylem vessel element length (L) and radius (R) corresponding to each analysed ultrasound pulse. Data from all three stem samples of H. quercifolia are merged here. The radii were obtained from the settling time of the ultrasound pulses, while the lengths were obtained from the resonance frequency of the sound pulses and by measuring the Young's modulus (Fig. 1e). The data points are classified into bins of L with intervals of 0.5 mm. In each bin, the median L and R are calculated (pink squares), and fitted with a power law function (blue line). The green dashed line indicates the predicted L-R dependency in accordance with Darcy-Weisbach equation for fluid flow, combined with mechanical failure of the xylem vessel (Methods). Red circles: observed vessel element lengths and radius in H. quercifolia via cryo-SEM technique.

Supplementary Files

This is a list of supplementary files associated with this preprint. Click to download.

- SUPPLI1.pdf